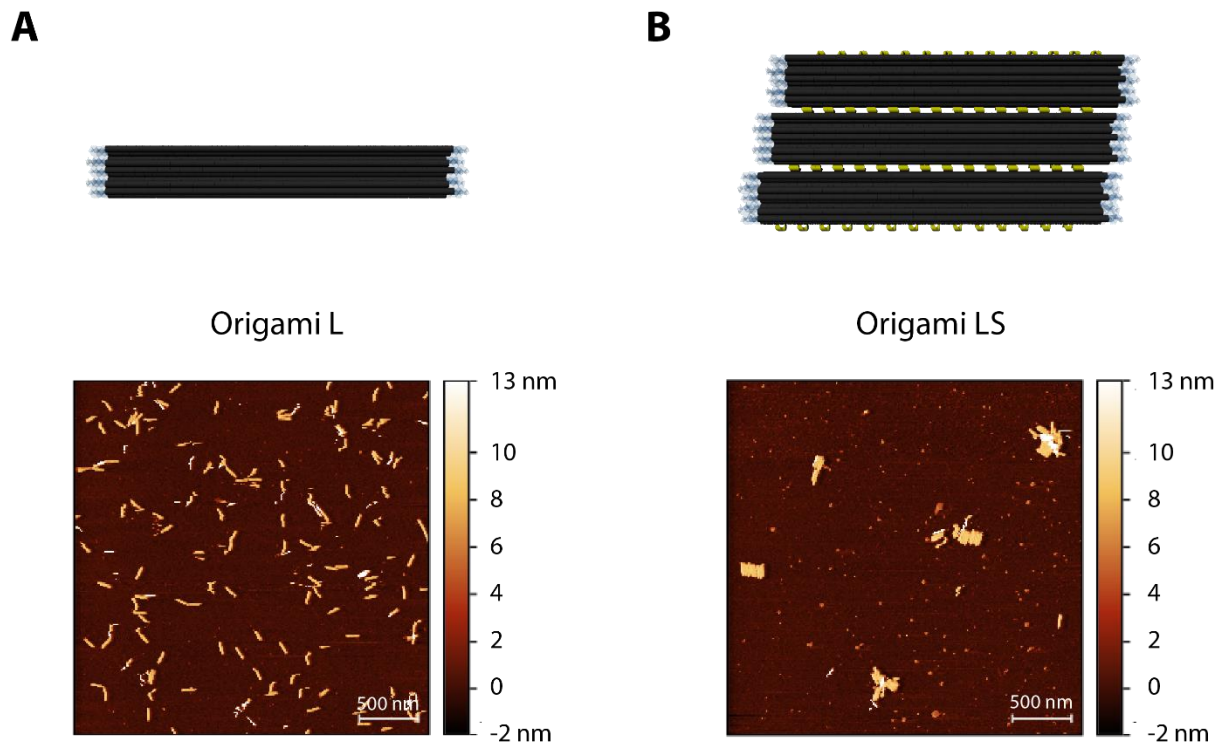


**Figure S2 | Depiction of the self-assembly patterns of origami L and LS upon increasing  $MgCl_2$ .**

(A) Origami L does not possess the ability to polymerize, as it lacks blunt ends or lateral overhangs for establishing intermolecular interactions. (B) Origami LS displays 14 lateral self-complementary single-stranded overhangs on both sides, and is therefore able to polymerize into sheet-like oligomers at high  $MgCl_2$  concentrations.



**Figure S3 | Self-assembly properties of origami L and origami LS at high MgCl<sub>2</sub>.**

Atomic force microscopy (AFM) images on PLL-mica of origami L lacking blunt ends (**A**) and origami LS displaying 14 lateral self-complementary single-stranded overhangs on both sides (**B**) after incubation with a high MgCl<sub>2</sub> buffer (70 mM MgCl<sub>2</sub> + 187.5 mM NaCl). As here depicted, whereas origami L (**A**) stays in a monomeric form, origami LS (**B**) polymerizes into sheet-like oligomers.

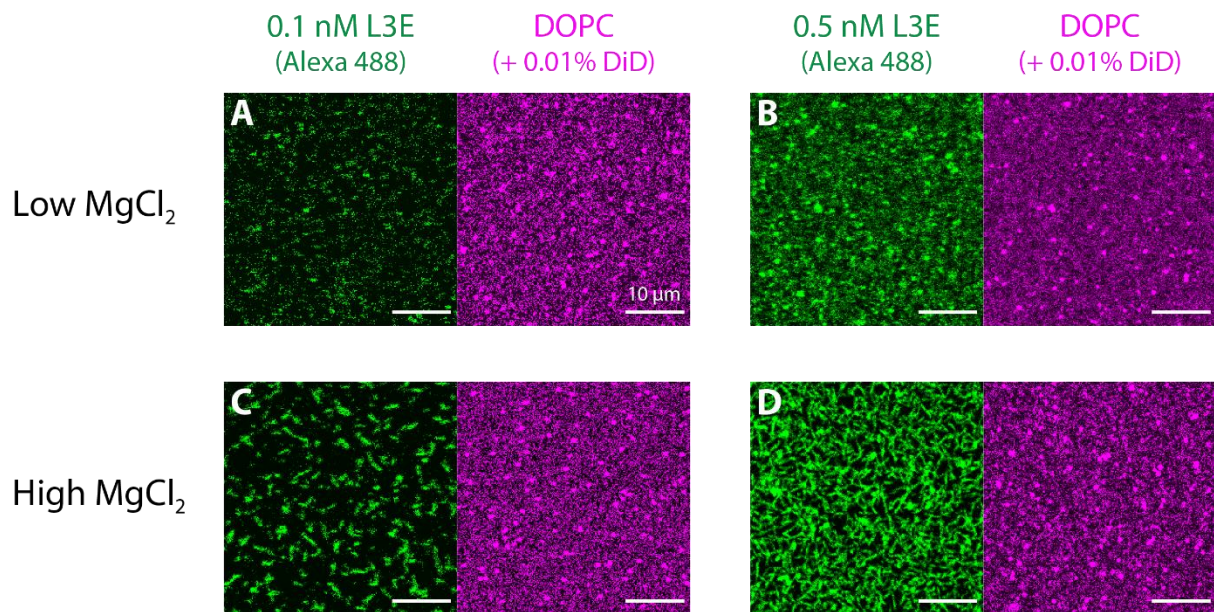


**Figure S4 | Binding and polymerization of DNA origami L3E on top of supported lipid bilayers.**

Zoomed-out images depicting the interaction of 0.1 and 0.5 nM Alexa488-labelled DNA origami L3E displaying 3 TEG-chol anchors (for membrane binding) and blunt ends (for end-to-end self-assembly) with DOPC SLBs (doped with 0.01% DiD). **(A-B)** At low  $\text{MgCl}_2$  (5 mM  $\text{MgCl}_2$  + 300 mM NaCl), a mostly homogenous distribution of origami L3E was observed on top of the lipid bilayers. **(C-D)** At high  $\text{MgCl}_2$  (70 mM  $\text{MgCl}_2$  + 187.5 mM NaCl) origami filaments were observed on top of the lipid bilayer. While at 0.1 nM, origami L3E formed individual short filaments **(C)**, at 0.5 nM origami L3E self-assembled into a mesh of longer and bundled filaments **(D)**.

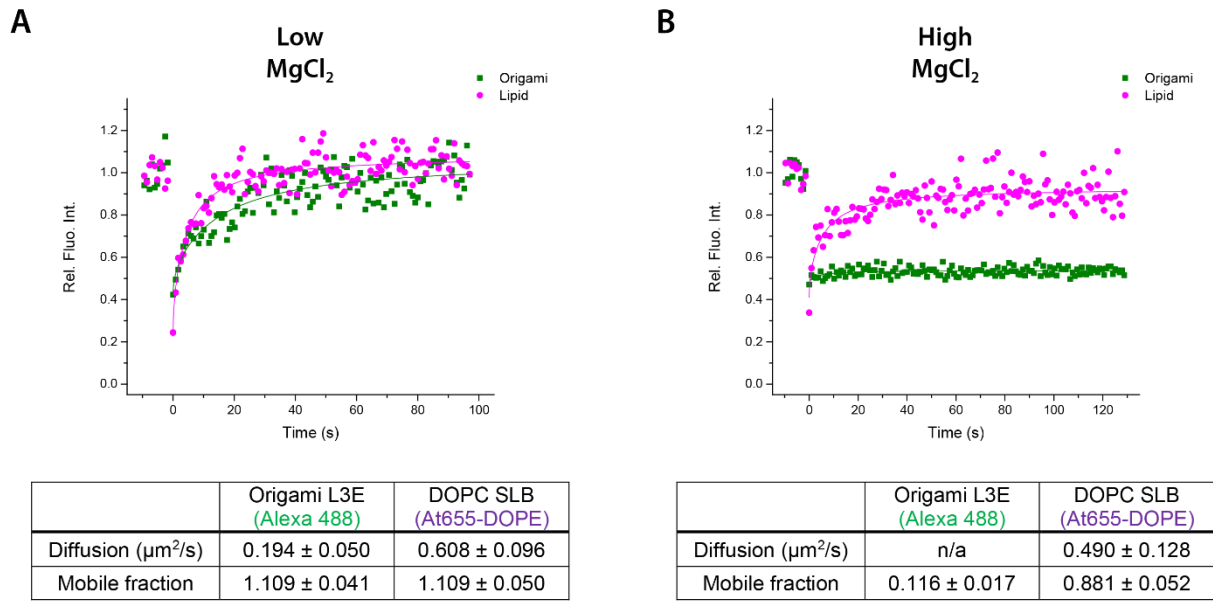


**Figure S5 | Fluorescence recovery after photobleaching (FRAP) of membrane-bound origami L3E on DOPC supported lipid bilayers (SLBs).**

FRAP data (from Movies S1 and S3), fitted results and calculated diffusion coefficients/mobile fractions of 0.5 nM origami L3E on a DOPC SLB, in the presence of **(A)** low MgCl<sub>2</sub> (5 mM MgCl<sub>2</sub> + 300 mM NaCl) and **(B)** high MgCl<sub>2</sub> (70 mM MgCl<sub>2</sub> + 187.5 mM NaCl).

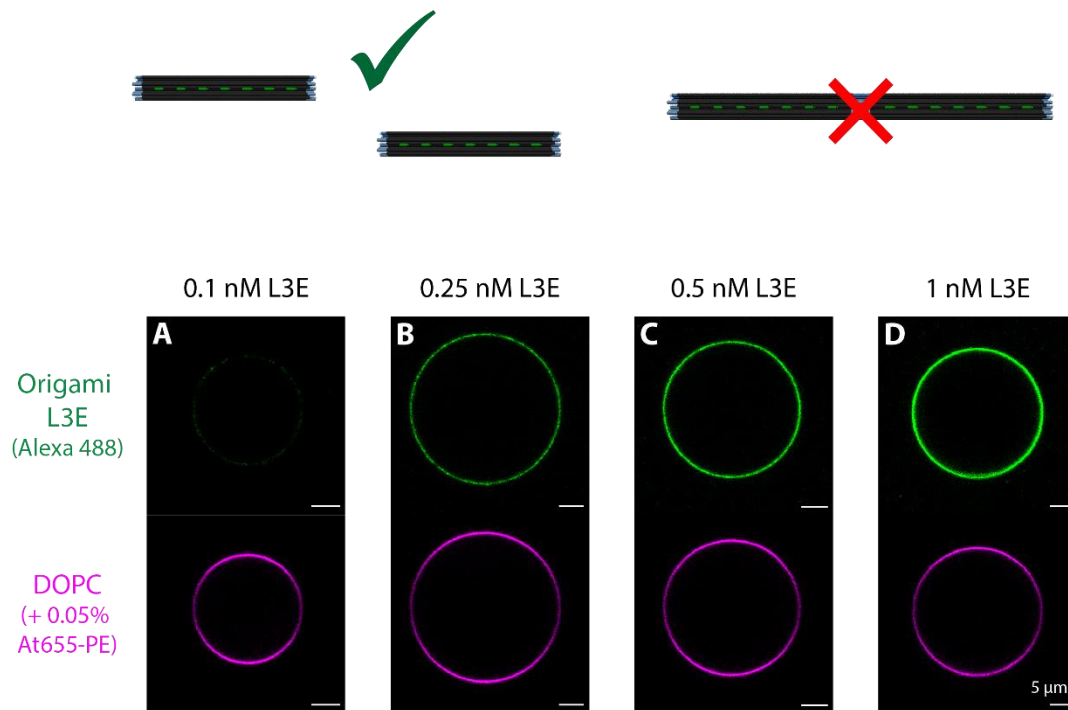


**Figure S6 | Interaction of origami L3E with giant unilamellar vesicles at low  $\text{MgCl}_2$ .**

Membrane attachment of different bulk concentrations (0.1-1 nM) of Alexa488/TEG-chol-modified origami L3E displaying blunt ends to DOPC GUVs (doped with 0.05% Atto655-DOPE) in the presence of low  $\text{MgCl}_2$  buffer (5 mM  $\text{MgCl}_2$  + 300 mM NaCl). Images correspond to equatorial plane slices of GUVs.

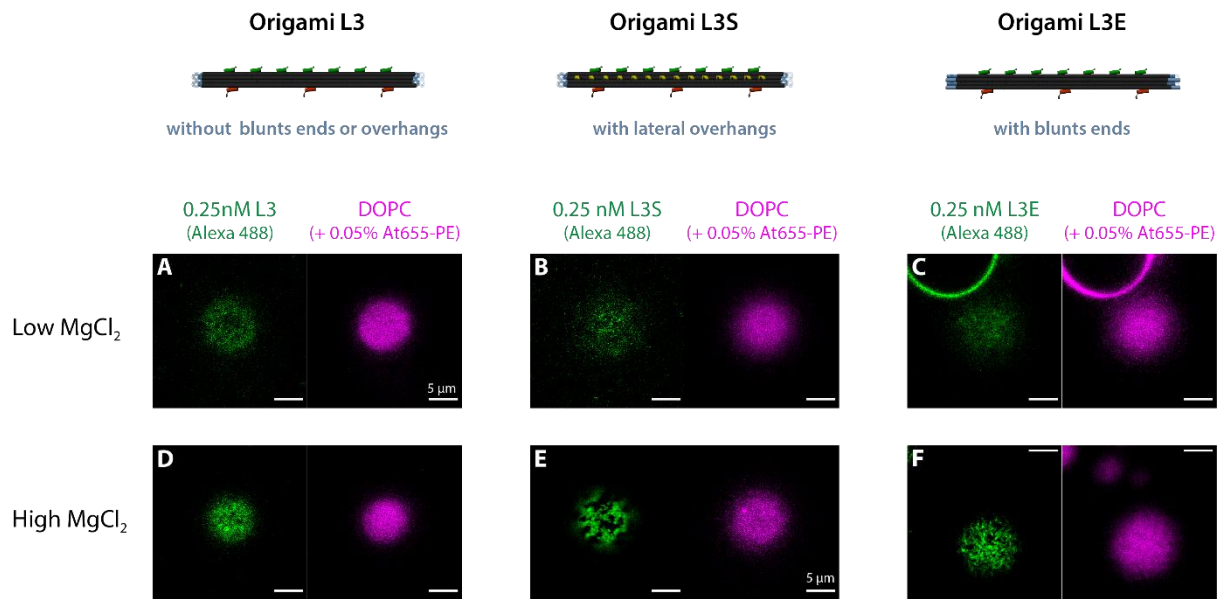


**Figure S7 | Triggering self-assembly of membrane-bound origami L3, L3S and L3E.**

As depicted for the pole of selected GUVs, at low  $\text{MgCl}_2$  (A-C), origami L3, L3S and L3E are homogeneously distributed on top of DOPC GUVs, corroborating their predominant monomeric state under these conditions. Upon increasing the amount of  $\text{MgCl}_2$ , membrane-bound origami L3 (lacking blunt ends and lateral overhangs) remains homogeneously distributed (D); origami L3S (displayed lateral overhangs) can engage into lateral self-assembly, giving rise to large platforms (E); and finally origami L3E (displaying blunt ends) can polymerize end-to-end, giving rise to a mesh of filaments (F).



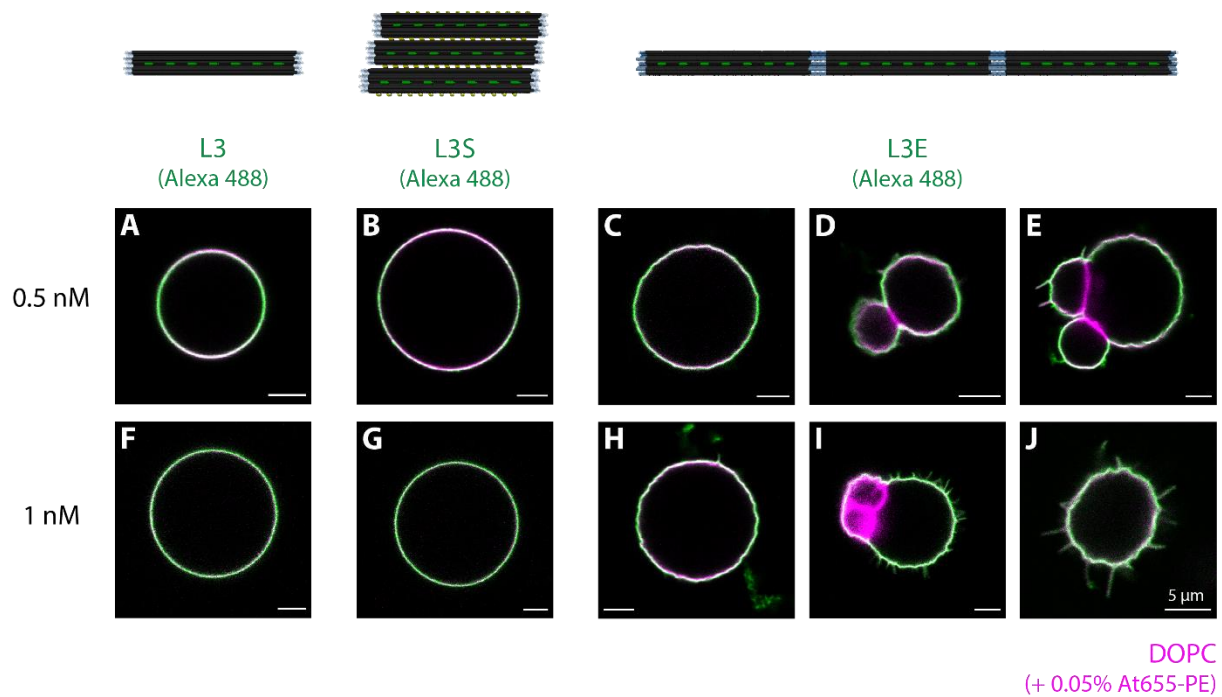


**Figure S8 | Membrane deformations by origami L3, L3S and L3E at high  $MgCl_2$ .**

Equatorial plane images of GUVs incubated with 0.5 nM (A-E) and 1 nM (F-J) origami L3/L3S/L3E at least 90 min prior addition of additional  $MgCl_2$ . For origami L3 lacking the ability to polymerize (A, F) no significant membrane deformations were reported. Similar results were observed for vesicles incubated with origami L3S, able to form lateral origami platform (B, G). On the contrary, for vesicles with membrane-bound origami L3E, extensive remodelling as rough (C, H) and spike-like **tubular** (D, E, I, J) deformations were observed, after  $MgCl_2$ -triggered end-to-end self-assembly of L3E into linear origami aggregates/filaments.



**Table S1 | List of functional staples used for various origami L structures.**

Oligo	Sequence	Description	Partner staple
TD_00	AAATTCGCCCGGAACAAAGAAAAAACACCAAACCC	staples with extension for Alexa488 dye	<i>5'-Alexa488-</i>
TD_01	ATTCATCTATACAAATTCTAAAAACACCAAACCC	<i>used in all origami</i>	<i>GGGTTTGGTGTTTTTT</i>
TD_02	ATTTATTTCCAATAATAAGAAAAAACACCAAACCC		
TD_03	AAGTGCCGTGGAAAGCGCAGTAAAAACACCAAACCC		
TD_04	CAAGATTTGTTAAAGGCCGCTAAAAACACCAAACCC		
TD_05	TTACTTCAAAAAACAAAATAAAAAACACCAAACCC		
TD_06	AGACAGGAAATGTGTAGGTAAAAAACACCAAACCC		
B18_00	ATTATCATCATAAACAGTATGGCTATGGGTGGTCTGGTT	staples with extension for TEG-Chol(18)	<i>5'-Chol-TEG-</i>
B18_03	GTAAGCGTCATGATTAGCACGCTATGGGTGGTCTGGTT	<i>used in origami L3, L3E and L3S</i>	<i>AACCAGACCCCATAGC</i>
B18_06	AAGGCCGGAGACATGTACCTCGCTATGGGTGGTCTGGTT		
E_02	TTAGAATCAGAGCGGG	staples for tip-to-tip blunt end interactions	
F_02	GCGGTTTGCGTATTG	<i>used in origami LE and L3E</i>	
E_03	AGCTAAACAGGAGGCC		
F_03	AACGCGGGGAGAG		
E_04	CCTGAGAAGTGTTTTATA		
F_04	GGGAAACCTGTCGTGC		
E_05	ATCAGTGAGGCCACCGAGT		
F_05	TGCCCGCTTTCAGTC		
E_07	TTAGTAATAACATCACTTG		
F_07	TAAAGCCTGGGGTGCC		
E_09	TACCGCCAGCCATTGC		
F_09	TGAAATTGTTATCCGCTCA		
E_12	GTAATAAAAGGGACATTCT		
F_12	TAAAACGACGGCCAGT		
E_13	GGCCAACAGAGATAGAACC		
F_13	CCCAGTCACGACGTTG		
E_14	CAGACAATATTTTGAATG		
F_14	TGTGCTGCAAGGCGAT		
E_15	GCTATTAGTCTTTAATGCG		
F_15	GCTGGCGAAAGGGGA		
E_17	GAAGATAAACAGAGG		
F_17	AGGCTGCGCAACTGTTGGG		
E_19	CTGAGAGCCAGCAGCA		
F_19	ACTCCAGCCAGCTT		
LS_00	TATATATTTAATTTACAATAGATAATACAT	staples for lateral oligomerization	
LS_01	TATATATTTAAGCAAAGCGCGCAGAGGCG	<i>used in origami LS and L3S</i>	
LS_02	TATATATTTCTACCGTGATCTTCTGACCT		
LS_03	TATATATTTACGGTATTAATAATCGGCTGT		
LS_04	TATATATTTAAGAATTAATAAACATAAAA		
LS_05	TATATATTTCCCGATTGATTACCAGCGCCA		
LS_06	TATATATTTCCGCCAGCATCAGAGCCGCCA		
LS_07	TATATATTTTCGGCCACCCATAGGTGATCA		
LS_08	TATATATTTTCTGATACCTCAGCTTGCTTT		
LS_09	TATATATTTATGCGCAGACCGGACCTGCT		
LS_10	TATATATTTAAAAATGCAGTCATCAGTTGAG		
LS_11	TATATATTTTATTAGAGAGAACCAGACCGG		
LS_12	TATATATTTTGACTTTTGAATCGGTTGTAC		
LS_13	TATATATTTCTTGTTAAAACGTTAATATTT		
RS_00	TATATATTTAAACCCTCAATCTTAGAACAA		
RS_01	TATATATTTTTCGGTAGATTTAGAAGAGTT		
RS_02	TATATATTTTAAACCTCCGGAGAATATCA		
RS_03	TATATATTTATAACAACATGCCAGCTCC		
RS_04	TATATATTTAGAGCCTAATTTATAACGGAG		
RS_05	TATATATTTTATGTTAGCAAAAGCGTCATT		
RS_06	TATATATTTATTAGCGTTTGCATAAACAAAT		
RS_07	TATATATTTGAAAGTATTAAGAGTAAATTC		
RS_08	TATATATTTAGCGGAGTGAGATAAACGGAA		
RS_09	TATATATTTAGAGGCAAAAGAAGTAGTAAA		
RS_10	TATATATTTTACCTTATGCGCCCTCAAAA		
RS_11	TATATATTTATCAGGTCTTTACGCAAAATCT		
RS_12	TATATATTTGAAAAGGTGGCAAGATCTAGA		
RS_13	TATATATTTGAATCGATGAACAGTTTGAGC		

**Table S2 | Fraction of deformed vesicles, upon increasing MgCl<sub>2</sub>, as a function of total L3E concentration.**

<b>[L3E] (nM)</b>	<b>% Deformed vesicles (± st. dev.)</b>	<b>Independent repeats</b>	<b>Total number vesicles (<math>N_{total}</math>)</b>
0.1	10.9 ± 10.1%	4	174
0.25	37.1 ± 20.9%	5	316
0.5	65.6 ± 12.1%	5	401
1	70.2 ± 9.6%	4	350

## Movie Captions

**Movie S1** | FRAP of 0.5 nM origami L3E (Alexa488-labelled, green) on top of DOPC SLB (doped with Atto655-DOPE, magenta), in the presence of a low  $\text{MgCl}_2$  buffer (5 mM  $\text{MgCl}_2$  + 300 mM NaCl). Corresponding data represented in Figure 3SA. Scalebar is 5  $\mu\text{m}$ .

**Movie S2** | Time-series of  $\text{MgCl}_2$ -triggered polymerization of 0.5 nM origami L3E (Alexa488-labelled, green) on top of DOPC SLB. Addition of  $\text{MgCl}_2$  happened at timepoint 5:00. Scalebar is 10  $\mu\text{m}$ .

**Movie S3** | FRAP of 0.5 nM origami L3E (Alexa488-labelled, green) on top of DOPC SLB (doped with DiD, magenta), in the presence of a high  $\text{MgCl}_2$  buffer (70 mM  $\text{MgCl}_2$  + 187.5 mM NaCl). Corresponding data represented in Figure 3SB. Scalebar is 5  $\mu\text{m}$ .

**Movies S4 & S5** | Diffusion of 0.1nM origami L3E (Alexa488-labelled, green) on the pole of GUVs (doped with Atto655-DOPE, magenta), after  $\text{MgCl}_2$ -mediated polymerization into membrane-bound end-to-end self-assembled filaments.

**Movie S6** | Diffusion of 0.1nM origami L3S (Alexa488-labelled, green) on the pole of GUV (doped with Atto655-DOPE, magenta), after  $\text{MgCl}_2$ -mediated polymerization into membrane-bound laterally self-assembled platforms.

**Movie S7** | Characteristic wrinkled membrane deformations on DOPC GUV (doped with Atto655-DOPE, magenta) induced by membrane-bound origami L3E (Alexa488-labelled, green) at 1 nM bulk concentration, after  $\text{MgCl}_2$ -mediated polymerization into filaments. Scalebar is 5  $\mu\text{m}$ .

**Movie S8** | Characteristic spike-like tubular deformations on DOPC GUV (doped with Atto655-DOPE, magenta) induced by membrane-bound origami L3E (Alexa488-labelled, green) at 1 nM bulk concentration, after  $\text{MgCl}_2$ -mediated polymerization into filaments. Scalebar is 5  $\mu\text{m}$ .